https://doi.org/10.5194/egusphere-2026-3968
Preprint. Discussion started: 17 August 2026

Evaluating the performance of the thermodynamic equilibrium model ISORROPIA 2.1 for different aerosol compositions

Irene Gini[1*], Mattia Borelli[2], Guido Pirovano[1], Alessandra Balzarini[1], Amedeo M. Cefalì[1], Ezio G. Bolzacchini[3], Andrea Doldi[3], Ludovica Giovanazzi[3], Niccolò Losi[3], Luca Ferrero[3]

[1]RSE S.p.A, Via Rubattino 54, Milan, 20134, Italy
[2]Department of Chemistry, University of Milan, Milan, 20133, Italy
[3]Department of Earth and Environmental Science, University of Milan-Bicocca, Milan, 20126, Italy

Correspondence to: Irene Gini (irene.gini@rse-web.it)

Abstract. The hygroscopic behavior of atmospheric aerosols is controlled by their chemical composition, which determines phase transitions, water uptake and physical state. Aerosol hydration influences particle size, mass, optical and chemical properties, making it a key process in atmospheric science. This study evaluates the performance of ISORROPIA 2.1, a thermodynamic equilibrium model, in predicting aerosol water uptake across a wide range of aerosol types, including indoor and outdoor (urban, extra-urban and marine) aerosols and deposits on electrical insulators. Inorganic composition was determined by ion chromatography, while deliquescence behavior was experimentally characterized using an Aerosol Exposure Chamber, providing a comprehensive dataset for model validation. ISORROPIA 2.1 accurately reproduces deliquescence relative humidity (DRH) and hygroscopic growth in sulfate–nitrate–ammonium dominated systems, with mean deviations of 4.3 ± 2.6 % RH for the onset of deliquescence (DRH_s) and 4.4 ± 3.2 % RH for completion (DRH_e). In contrast, ammonium-poor mixtures enriched in alkali and alkaline-earth ions (K^+, Mg^{2+}, Ca^{2+}, Na^+), including marine aerosol and insulator deposits, show non-physical humidification behavior characterized by discontinuous liquid–solid transitions. These anomalies arise from routine-selection instabilities in dust-rich regimes. Targeted code refinements improved model stability and water-uptake predictions, extending the applicability of ISORROPIA 2.1 to sulfate-poor, sodium- and crustal-rich systems. Overall, this work provides an experimental benchmark for aerosol thermodynamics, identifies the compositional limits of ISORROPIA 2.1 and broadens its applicability to complex inorganic aerosol mixtures.

https://doi.org/10.5194/egusphere-2026-3968
Preprint. Discussion started: 17 August 2026

1 Introduction

Atmospheric aerosol particles play a central role in many processes which can cause damaging effects on the environment and society (Makar et al. 2003). Their presence affects a broad range of atmospheric aspects (Neuberger et al. 2025) such as reduced visibility in highly polluted areas (Liu et al. 2022), formation of acid rain, alteration of the Earth's radiative balance (Calvin et al. 2023; Ferrero et al. 2018, 2021), thereby influencing climate change (Nenes et al., 1998). They also interfere with various human activities and technological systems (Wang et al. 2025; D'Angelo et al. 2017; Shehabi et al. 2008; Syed 2006; Litvak et al. 2000), extending their impact well beyond the atmospheric domain.

In all the aforementioned contexts, a central factor controlling the behavior and impacts of aerosol particles is their interaction with water. Water uptake influences particles' size and mass and their atmospheric lifetime (Pöschl 2005), the concentration of water–soluble compounds, optical properties, chemical reactivity, the effectiveness in acting as cloud condensation nuclei. In addition, aerosol hygroscopicity is highly relevant in cultural heritage context: the presence of liquid water can promote decay processes such as solid-liquid reactions, acid attack, penetration of salts solutions into porous materials. Moreover, phase transition cycles of aerosol can expose the cultural heritage works to mechanical decay (Casati et al. 2015). The aerosol hydration state is relevant in energy applications, particularly those involving energy distribution and electronic systems reliability. For example, hydrated atmospheric aerosols may endanger electronic components, by inducing electrochemical corrosion, electrical bridging and heat accumulation on electronic circuitry (D'Angelo et al. 2017; Ferrero et al. 2020). Atmospheric pollution also affects the performance of high-voltage insulators and can endanger the stability of the electric power system: under high ambient humidity, soluble compounds accumulated on the insulator surfaces can dissociate into ions, imparting conductivity to the polluted layer and potentially leading to flashover phenomena (Gini et al. 2023). Lastly, even in the medical and toxicological fields, hygroscopic properties are of great importance. The toxicity of suspended particles depends on particle size and chemical composition: smaller particles can penetrate deeper into the respiratory system, carrying potentially harmful substances. The same principle can be leveraged to optimize therapies based on nebulization administration (Haddrell et al. 2017).

Therefore the knowledge of the physical state, and of the hydration level of atmospheric aerosol, are fundamentals and depend on the relative humidity (RH) to which an aerosol particle is exposed; particularly, once the aerosol chemical composition is fixed, the aerosol physical state evolves accordingly to the RH history experienced in the atmosphere with respect to the values of the aerosols' deliquescence relative humidity (DRH) and crystallization relative humidity (CRH) (both chemically dependent; (Martin 2000). During a humidification process (i.e. an increase in RH), the aerosol is solid until RH reaches DRH: the aerosol starts to absorb water, producing a saturated aqueous solution; a further increase in the ambient RH leads to a complete dissolution of soluble components and hygroscopic growth due to the continuous condensation of water on the particles. The reverse happens during dehumidification (i.e. a reduction in RH starting from a value above the DRH): evaporation takes place and the aerosol particle remains supersaturated until the CRH (lower than DRH) is reached and crystallization occurs, leading once again to a dry state through a hysteresis cycle (Martin 2000; Martin et al. 2003; Seinfeld

https://doi.org/10.5194/egusphere-2026-3968
Preprint. Discussion started: 17 August 2026

and Pandis 2006). Therefore, DRH and CRH values determine whether in certain atmospheric conditions aerosol particles are solid or liquid (i.e. their soluble components are in solution) leading to an aerosol hydration hysteresis cycle (D'Angelo et al. 2016; M. Tang et al. 2019; Ferrero et al. 2020). Since the hydration state of atmospheric aerosols is strictly linked to its chemical composition, jointly understanding both properties is crucial (Berman et al. 2022).

The origin and the atmospheric evolution are fundamental in determining the aerosol chemical composition at a given site as atmospheric aerosols originate from both natural and anthropogenic sources (Fuzzi et al. 2015). They can be classified as primary, directly emitted into the atmosphere from different sources such as biomass burning, road transport, industrial activities, volcanic eruptions, wind-driven or traffic-related suspension of road, soil and mineral dust, sea salt, biological material (Pöschl 2005), or as secondary particles, formed in the atmosphere through gas–to–particle conversion of gaseous precursor (Seinfeld and Pandis 2006). Therefore, atmospheric aerosol is made up of a mixture of different components that can include inorganic salts, organic compounds, elemental carbon, crustal material, and various trace metals as well as water (Kim et al. 1993a; Kakavas et al. 2022). Inorganic salts typically account for 25–50 % of the aerosol mass, with dominant ions including sulfate (SO_4^{2-}), bisulfate (HSO_4^-), nitrate (NO_3^-), chloride (Cl^-), ammonium (NH_4^+), sodium (Na^+), potassium (K^+), magnesium (Mg^{2+}) and calcium (Ca^{2+}), with relative abundances varying with geographical location, time, meteorological conditions and particle size (Tsimpidi et al. 2025; Pöschl 2005; Heintzenberg 1989) strongly affecting DRH and CRH values. As each chemical species is characterized by a specific DRH and CRH; as an example, Martin (2000), reported the DRH and CRH of Na_2SO_4/H_2O system (84 % and 57 % RH respectively) which is different from the DRH and CRH of $NaCl/H_2O$ system (75 ± 1 % and 43 ± 2 % RH respectively). Several studies investigated the DRH and CRH of both single aerosol components (i.e. $(NH_4)_2SO_4$, NaCl, NH_4NO_3) and chemically complex aerosol systems (Kelly et al. 2014; D'Angelo et al. 2016; Cheung et al. 2020; Haddrell et al. 2017), highlighting how the chemical composition (especially the relative chemical composition of a internally mixed atmospheric aerosol) influences its phase transitions by affecting the DRH and CRH values.

In this respect, the inorganic chemical composition is enough to predict the DRH at the thermodynamic equilibrium using several models (e.g. E-AIM, ISORROPIA 2.1) (Ferrero et al. 2015), while it is not enough to predict the CRH. As Martin (2000) pointed out, the presence of metal oxides (i.e. Fe_2O_3, TiO_2…) in the aerosol's particles can lead to a CRH increase up to 32% more compared to a pure saline aerosol (i.e. pure $(NH_4)_2SO_4$), because such oxides can act as crystallization nuclei driving heterogeneous nucleation, which results in crystallization at higher RH values. Furthermore, the presence of organic material, such as glycerol or certain carboxylic acids, can also increase the aerosol's CRH (Choi and Chan 2002).

Focusing on the DRH only, models able to predict the composition and the physical state of aerosol over a wide ranges of temperatures and relative humidity have to deal with wide range of possible combination of inorganic ions; these models, in fact, are essential to understanding aerosol behavior in the atmosphere as aforementioned at the beginning (Wexler and Clegg 2002).

To compute the composition and phase state of aerosol, every aerosol model needs to know the thermodynamic equilibrium state, because the driving force for mass transfer of species between gas and aerosol phases is the departure from equilibrium (Nenes et al. 1998). However, this is a complex computational problem because of the solution of several nonlinear algebraic

https://doi.org/10.5194/egusphere-2026-3968
Preprint. Discussion started: 17 August 2026

equations or the minimization of the free energy of the gas–particle system (Nenes et al. 1999). Several thermodynamic equilibrium models have been developed over the last decades, treating different sets of aerosol components, and using different thermodynamic and numerical approaches (Clegg et al. 1992; Kim et al. 1993a, 1993b; Kim and Seinfeld 1995; Meng et al. 1995; Nenes et al. 1998, 1999; Ansari and Pandis 1999; Wexler and Clegg 2002; Metzger, Dentener, Pandis, et al. 2002; Metzger, Dentener, Krol, et al. 2002; Makar et al. 2003; Metzger et al. 2006).

However, despite the aforementioned efforts and considering the role of inorganic ions, some alkaline cations such as K^+, Mg^{2+} and Ca^{2+} (e.g. coming from dust and sea salt among other sources) exhibit a physicochemical effect on the aerosol water uptake that are not well understood yet (Kelly et al. 2014). For example, carbonates containing mineral dust particles (such as $CaCO_3$ and $CaMg(CO_3)_2$) have low hygroscopicity, but when they react with acidic gases in troposphere can form Ca- and Mg-containing salts with higher hygroscopicity, such as $Ca(NO_3)_2$ and $Mg(NO_3)_2$ (Guo et al. 2019). The alkaline cations are also an important part of sea salt aerosol (that includes Cl^-, Na^+, SO_4^{2-}, Mg^{2+}, Ca^{2+} and K^+); NaCl accounts for ~ 80 % of sea salt by mass, followed by $MgCl_2$, the second most abundant component, which plays a key role in the hygroscopic behavior of sea spray aerosol together with $CaCl_2$ (Gupta et al. 2015; Zieger et al. 2017).

The present work focuses on the performance and optimization of the thermodynamic model ISORROPIA 2.1, which predicts the physical state and composition of inorganic aerosol, starting from the concentrations of some aerosol precursors (NH_3, Na^+, Ca^{2+}, K^+, Mg^{2+}, HNO_3, HCl, H_2SO_4).

ISORROPIA 2.1 is more comprehensive than others (i.e. ISORROPIA1.7), since it considers alkali and alkaline earth metals (AAEMs) such as K^+, Mg^{2+} and Ca^{2+}. Hence, ISORROPIA 2.1 (hereafter abbreviated as ISORROPIA) is widely used in atmospheric chemistry to model aerosol behavior and is commonly integrated into several major chemistry–transport models, such as WRF-Chem , CMAQ (Wang et al. 2012), CHIMERE (Couvidat et al. 2018), GEOS-Chem (Pye et al. 2009; Norman et al. 2025) to provide a consistent treatment of inorganic aerosol thermodynamics. Given this widespread use, it is important to evaluate both the strengths and limitations of ISORROPIA across chemically distinct regimes.

In this work, the performance of ISORROPIA is investigated by applying it to different aerosol datasets with different characteristics: (1) indoor atmospheric aerosol; (2) outdoor atmospheric aerosol (urban, extra-urban and marine sites); (3) deposit of aerosol on insulators surfaces; (4) synthetic aerosol (pure salts). The four datasets in fact enable to distinguish several situations in which the performance of ISORROPIA changes as a function of the aerosol chemical composition, highlighting both its strengths and weaknesses. Among these datasets, the one representing aerosol deposits on insulators surfaces, is particularly valuable for its relevance to national power-system resilience in an increasingly electrified context. The chemical composition of deposits, rich in AAEMs, such as Na^+, K^+, Mg^{2+}, Ca^{2+}, differs from the typical chemical composition of atmospheric aerosols, which is generally dominated by sulfates, nitrates and ammonium in varying proportions depending on season and location. This chemical scenario is not unique to deposits on electrical insulators, but is common in many atmospheric contexts: Chithra and Shiva Nagendra (2013) highlight relevant concentrations of K^+, Mg^{2+} and Ca^{2+} in indoor school environments due to soil resuspension; at industrial and marine sites, PM is frequently enriched in AAEMs (Chianese

https://doi.org/10.5194/egusphere-2026-3968
Preprint. Discussion started: 17 August 2026

et al. 2022) and these species are extensively mobilized in the atmosphere during industrial (Ruan et al. 2024) and biomass (Dalkhsuren et al. 2023; W. Cheng et al. 2024) combustion processes. Specific studies on emissions processes confirm the strong tendency of AAEM salts to migrate into the aerosol phase: for example, Cheng et al. (2025) show that the addition of NaCl during combustion leads to the formation of submicron particles consisting almost entirely of alkali chlorides; Lei et al. (2022) point out that the presence of H_2O in the combustion stream can alter the volatilization of AAEMs, resulting in an enrichment of Na^+, K^+, Mg^{2+}, Ca^{2+} in ultrafine PM. Jabłońska et al. (2021) demonstrate that inhaled PM consists primarily of calcium and magnesium carbonates, indicating that Ca^{2+} and Mg^{2+} are common components of urban aerosols. Furthermore, Zhang et al. (2020) show that Na^+ and K^+ play a key role in the hygroscopic growth of saline dust and sea-salt aerosols, with dust particles rich in AAEMs absorbing significant amounts of water at high RH, thus requiring careful treatment of their hygroscopicity in models.

The experimental setups and the sampling campaigns associated with each aerosol dataset are described in detail in Sect. 2, with particular focus on the instrumentation used and sampling campaigns characteristics. Specific methodologies were employed for the chemical analyses of samples and for the identification of their thermodynamic behavior. Section 3 presents the application of ISORROPIA to the different datasets, with the aim of evaluating its performance in simulating the thermodynamic behavior of atmospheric aerosols. This Section outlines the simulation results, comparisons with experimental references, and an evaluation of model performance under different chemical conditions, discussing agreements or deviations between predictions and observations. This multi-scenario approach allows a comprehensive assessment of ISORROPIA's robustness and limitations, as summarized in Sect. 4.

2 Material and methods

Several sampling campaigns were carried out at various sites with different characteristics. The specific features of each site, along with the sampling methodology, are described below.

The study involved the collection of aerosol samples in different environmental contexts and characterized by different chemical properties: (1) indoor aerosol dominated by sulfates (Subsect. 3.1); (2) outdoor aerosol collected in urban and extra-urban sites (dominated by nitrates) and marine site (dominated by sodium chloride) (Subsect. 3.2); (3) aerosol deposited on the surface of insulators belonging to the Italian electrical network, characterized by the presence of sodium and crustal element (Subsect. 3.3); (4) synthetic aerosol with a controlled chemical composition (pure salts, e.g. $MgCl_2$, $Ca(NO_3)_2$) (Subsect. 3.4). The aerosol collected on filters was chemically characterized through Ion Chromatography (IC, Subsect. 2.3) and thermodynamically characterized in Aerosol Exposure Chamber (AEC, Subsect. 2.5). For air-sampled aerosols, the thermodynamic hysteresis cycle was identified directly on the filter, while for deposits samples it was necessary to reproduce the aerosol in laboratory and deposit it on Teflon filters for the analysis in AEC. This thermodynamic characterization was fundamental in building a robust experimental dataset to validate ISORROPIA. The present paper focuses on the application of ISORROPIA to these different case studies. Thanks to the availability of both chemical and thermodynamic data, the model

https://doi.org/10.5194/egusphere-2026-3968
Preprint. Discussion started: 17 August 2026

could be evaluated under a variety of chemical conditions, with particular attention to how its performance varies as a function of aerosol chemical composition.

2.1 Sampling campaigns

Aerosol samples were collected both outdoors and indoors to have at disposal a wide range of particles chemical composition to test the performance of ISORROPIA on different case studies.

Ordering them by sampling dates, the samples collected are the following ones:

1) During the winter of 2016, a sampling campaign was carried out at Milano-Malpensa Airport (MXP); the campaign ran from September 2016 to February 2017, collecting 128 PM_{10} samples. Twelve of these were analyzed for their chemical composition through IC and for their hygroscopic behavior using the AEC.
2) Marine samples were collected close to Barbados during the EUREC^{4}A (ElUcidating the RolE of Cloud-Circulation Coupling in ClimaAte) project (Stevens et al. 2021), which is an international initiative in support the World Climate Research Program's Grand Science Challenge on Clouds, Circulation and Climate Sensitivity. EUREC^{4}A took place between 20 January and 20 February 2020 on board of the French ship ATLANTE. During this period aerosol samples were collected by means of a total suspended particulate sampler (ECHO-PUF, Subsect. 2.2): 23 samples were collected and 11 of these were collected on Teflon filters (porosity 2 µm) with 5 filed blanks. A Ø = 47 mm punch for each sample was token and chemical characterized through an IC system and analyzed in AEC.
3) Indoor aerosol samples ($PM_{2.5}$) were collected during a campaign carried out in 2020–2021, within two rooms (ROOM 1 and ROOM 2) of a Data Centre (DC) located in the Po Valley (Ferrero et al. 2013). The campaign involved filters collection during both summer period (July 2020) and winter period (January 2021). Summer and winter samples collect on Teflon filters (Ø = 47 mm, porosity 2 µm) through the HYDRA Dual Sampler (Subsect. 2.2) were analyzed through an IC system and AEC.
4) In December 2022, a 22-days sampling campaign (December 6th–27th, 2022) was conducted at the sampling site of the Atmospheric Chemistry Laboratory of the University of Milano-Bicocca (UNIMIB-U9), which is an urban background site. The campaign involved the use of 10 Teflon filters (Ø = 47 mm, porosity 2 µm), sampled for 24 hours every three days, through the HYDRA Dual Sampler; two of them were used as field blanks. The collected aerosol was chemically characterized by IC and AEC.
5) Finally, during 2016–2018 a sampling campaign, involving collecting aerosol deposits on the surface of Italian electric network's insulators, was carried out. The collection of aerosol samples on insulators followed the swab technique explained in the Technical Specification (IEC 60815-1). The pollutants were wiped out from the insulator surface with a squeezed sponge, previously wetted with distilled water; then the pollutants were dissolved into 1L of distilled water by shaking and squeezing the sponge in the water. Based on the chemical analyses of the samples collected during the campaign, the Italian territory was divided into three macro-regions (MR): macro-region 1 (MR1, Sardinia and Sicily), macro-region 2 (MR2, south-western regions) and macro-region 3 (MR3, north-eastern regions).

https://doi.org/10.5194/egusphere-2026-3968
Preprint. Discussion started: 17 August 2026

All the samples were chemically characterized by IC in order to synthetically reproduce their chemical composition in laboratory, using an aerosol generation system (Section 2.4), and to carry out the studies in AEC. The detailed procedure is explained in Gini et al. (2023) and MRs definition is shown in the supplementary materials, Figure S1.

The five ensembles of aerosol samples enabled assessing the performance of ISORROPIA on different chemical aerosol compositions.

2.2 Sampling techniques

To collect the aerosol sample on filter, a two-channel PMx sampler model HYDRA Dual Samples (FAI Instruments) was used. The instrument is an automatic sequential low volume sampler enabling collecting aerosol particles (suspended in the atmosphere) on 47 mm Teflon filter membranes, with two independent sampling lines, equipped with a specific sampling head (e.g. PM_{10}, $PM_{2.5}$). Each sampled filter was analyzed both in IC, to determine the inorganic ionic composition of collected aerosol, and in AEC, to identify the hysteresis cycle of the aerosol focusing on the DRH.

Only during the EUREC^{4}A campaign, another sampling system was used: the high-volume sampler ECHO-PUF (TCR, Tecora, Milan, Italy, Fig. S2): it enabled to the collection of total suspended particulate (TSP). The sampler was equipped with a filter holder for collecting TSP on Teflon membrane filters with a diameter of 102 mm at a flow rate of 200 L min^{-1}, to minimize the sampling artefacts (sorption of gases on the filter and the volatilization of particle-bound compounds form the filter), with an average sampling time of 24 hours per filter. Once sampled filters were stored in aluminum foils at –20°C in the dark, until analysis. Before and after sampling, the filters were equilibrated (48 h at 10% RH, room temperature) and weighted with a microbalance (1 µg precision, model M5P-000V001; Sartorius, Göttingen, Germany) in order to measure the collected mass of TSP.

2.3 Ion Chromatography (IC)

The collected aerosol samples were analyzed by using a coupled ion chromatography system (Dionex ICS-90 and Dionex ICS-2000). The system has been equipped with an AS3000 Autosampler to identify the ionic inorganic fraction of the aerosol collected or deposited on the filters. For IC analysis, samples were extracted in a known volume (i.e. 3 mL) of ultrapure water (Milli-Q; resistivity 18.2 MΩ · cm at 25 °C) with a 20 minutes ultrasonic bath (SOLTEC SONICA®) and then the obtained solutions were filtered (0.45 µm PTFE membrane, 15 mm Syringe Filters, Alltech, Nicholasville, KY, USA) to remove any possible solid particle in suspension that would damage the chromatographic system. Anions (F^-, Cl^-, NO_3^-, SO_4^{2-}, PO_4^{3-}) were analyzed with a Dionex Ion Pac AG11 (4 x 50 mm) and AS11 (4 x 250 mm) guard and analytical columns in gradient elution, from 0.1 to 50 mM of KOH (KOH EGC II cartridge) to a flow rate of 0.8 mL/min. The electrical signal of the eluent was lowered by means of chemical suppressor (Dionex AMMS III 2 mm MicroMembrane Suppressor, regenerant solution: H_2SO_4, 0.05 M, Fluka 84720). Cations (Na^+, NH_4^+, K^+, Mg^{2+}, Ca^{2+}) were analyzed with a CG12A-5 µm and CS12A-5 µm guard and analytical columns by an isocratic elution of MSA (methanesulfonic acid, CH_3SO_3H, 20 Mm, Fluka 64280) at a flow rate of

https://doi.org/10.5194/egusphere-2026-3968
Preprint. Discussion started: 17 August 2026

0.5 mL/min. The signal of the eluent was reduced with a chemical suppressor (Dionex CMMS III 4 mm MicroMembrane Suppressor, regenerant solution: tetrabutylammonium hydroxide, TBA-OH, 0.1 M, Fluka). The quantification was performed using the external standard method by means of liquid standards (1000 g/L, Fluka, Sigma-Aldrich, St. Louise, MO, USA). The methodology used is described and validated in (Ferrero et al. 2015, 2018).

2.4 Aerosol Generator System

In order to investigate the phase transitions of the aerosol collected on insulators surface, not only ambient aerosol samples were investigated but synthetic aerosol with the same chemical composition of the aerosol deposited on the insulators was generated through an aerosol generation system (Aerosol Generator ATM 220, Topas GmbH; mini-AEC, 50 L volume, TEFLON® FEP type 200 A, thickness 50 µm; Mega System pump) (supplementary materials, Fig. S3).
On the basis of the chemical composition revealed by analyses for the MRs obtained via IC (section 2.3), 10000 ppm saline aqueous solutions for each MR were prepared and used for synthetic aerosol generation. The generated aerosol was deposited on PTFE filters (Ø = 47 mm, porosity 2 µm) which were used for the identification of the phase transitions in AEC (Gini et al. 2023).

2.5 Aerosol Exposure Chamber (AEC)

The Aerosol Exposure Chamber (AEC) is a sealed 1 m^3 glass chamber (Casati et al. 2015; Ferrero et al. 2015; D'Angelo et al. 2016; Ferrero et al. 2020; Gini et al. 2023) (supplementary materials, Fig. S4) covered by a polyurethane layer in which the samples are exposed to humidification and dehumidification cycles, from 20% to 90% RH and vice versa, with RH steps of 2%. During the humidification phase ultrapure water vapor (Milli-Q®; 18.2 MΩ · cm at 25 °C) was introduced into the chamber to raise the RH; conversely, during dehumidification phase, pre-filtered pure air (Aria Zero®, Sapio, Monza, Italy) was introduced in the AEC to reduce the RH. The increasing (or decreasing) mass measurements of the Teflon filter with the aerosol on as the RH varied were recorded by using an analytical balance (Sartorius SE-2F; accuracy ± 0.1 µg). The deliquescence and crystallization regions were determined according to the gradient method (Ferrero et al. 2015; D'Angelo et al. 2016), which further details are presented in the supplementary materials (Fig. S5). Since ISORROPIA can simulate only the deliquescence process, the present work focuses on this transition phase, especially on the starting (DRH_s) and ending (DRH_e) point of the deliquescence. It is noteworthy that, being the AEC experimental results, the phase transitions are by definition due to the synergy among the whole ensemble of chemical species in the aerosol samples; therefore, the obtained results represent the so-called mutual DRH often reported as MDRH (Martin, 2000).

2.6 ISORROPIA

The experimental results were compared against ISORROPIA vers. 2.1 (Fountoukis and Nenes 2007; Nenes et al. 1998, 1999), a thermodynamic model able to predict the physical state and composition of inorganic atmospheric aerosol. ISORROPIA models the sodium–ammonium–chloride–sulfate–nitrate–calcium–potassium–magnesium–water system, modelling its

https://doi.org/10.5194/egusphere-2026-3968
Preprint. Discussion started: 17 August 2026

partitioning between gas, liquid and solid phases. Thus, the model is capable of predicting the equilibrium composition of multicomponent inorganic aerosol under varying ambient temperature and relative humidity conditions.

The model defines 5 aerosol composition regimes based on the values of "*total sulfate ratio*" (R_1), "*crustal species and sodium ratio*" (R_2) and "*crustal species ratio*" (R_3) (Fountoukis and Nenes 2007). These ratios are calculated starting from the molar concentrations of aerosol precursors involved in sulfate neutralization, according to the following expressions (Eq. (1), Eq. (2), Eq. (3)).

$$R_1 = \frac{[NH_4^+]+[Ca^{2+}]+[K^+]+[Mg^{2+}]+[Na^+]}{[SO_4^{2-}]} \quad (1)$$

$$R_2 = \frac{[Ca^{2+}]+[K^+]+[Mg^{2+}]+[Na^+]}{[SO_4^{2-}]} \quad (2)$$

$$R_3 = \frac{[Ca^{2+}]+[K^+]+[Mg^{2+}]}{[SO_4^{2-}]} \quad (3)$$

Based on the values of these ratios, the model identifies:

- Sulfate super-rich (free acid) system (R_1<1): sulfates are in excess and not fully neutralized, with part of them present as free sulfuric acid. These conditions always lead to a liquid phase, as sulfuric acid is extremely hygroscopic.
- Sulfate rich (non-free acid) system (1≤R_1<2): there is sufficient ammonia and sodium to partially neutralize sulfates, which are present as a mixture of bisulfates (HSO_4^-) and sulfates (SO_4^{2-}), with their ratio determined by the thermodynamic equilibrium.
- Sulfate poor, crustal and sodium poor (R_1≥2, R_2<2): sulfates are fully neutralized by ammonia and partially by sodium and crustal cations. However, sodium and crustal cations are not sufficient to fully account for neutralization. Excess ammonia can react with HNO_3 and HCl, leading to the formation of volatile salts (NH_4NO_3, NH_4Cl).
- Sulfate poor, crustal and sodium rich, dust poor (R_1≥2, R_2≥2, R_3<2): there is sufficient sodium and crustal cations to fully neutralized sulfate, but the amount of crustal species alone is insufficient to form crustal nitrates and chlorides (e.g. $Ca(NO_3)_2$, $MgCl_2$). Sodium and ammonia may still react with HNO_3 and HCl to form NH_4NO_3, NH_4Cl, $NaNO_3$ and NaCl.
- Sulfate poor, crustal and sodium rich, dust rich (R_1≥2, R_2≥2, R_3>2): there is an abundance of crustal cations, sodium and ammonia. Sulfates are fully neutralized, and the system can support the formation of nitrate and chloride salts with all types of cations, including crustal species (e.g. $Ca(NO_3)_2$, $CaCl_2$, $Mg(NO_3)_2$, $MgCl_2$, KNO_3, KCl).

These parameters together with RH, temperature and the relative abundance of each aerosol precursor (NH_3, Na^+, Ca^{2+}, K^+, Mg^{2+}, HNO_3, HCl, H_2SO_4), determine the appropriate set of equilibrium, mass conservation, electroneutrality and water activity equations.

The aerosol can be either in a thermodynamically stable state, where salts precipitate if saturation is exceeded, or in a metastable state, where salts do not precipitate under supersaturated conditions. ISORROPIA also includes the treatment of the MDRH

https://doi.org/10.5194/egusphere-2026-3968
Preprint. Discussion started: 17 August 2026

of multicomponent salt particle solutions. Soluble particles transform into an aqueous solution when the relative humidity reaches the MDRH; the MDRH of a salt mixture depends upon the mixture composition and is always lower than the minimum DRH of each component (Martin 2000). Given that, for simplicity the acronym DRH will be hereinafter used; it is understood that when it is referred to an ambient aerosol sample, it is related to the feature of the chemical mixture of each sample.

To perform the simulations presented in Sect. 3, ISORROPIA was used in reverse mode, which considers the concentrations of the input species in the aerosol phase, in order to simulate the experimental outcomes obtained with the AEC. The input concentrations used to simulate the humidification phase with ISORROPIA were the inorganic concentrations of the collected samples identified by IC system. Since in the case studies all major inorganic species were present, ISORROPIA simulated an ammonium–sulfate–nitrate–chloride–sodium–calcium–potassium–magnesium aerosol system, with the composition regime determined by sulfate and sodium ratios and by the ambient relative humidity.

3 Results and discussion

In this section, the results, obtained from modelling the thermodynamic behavior of the collected aerosol in different contexts (with different chemical composition), are presented. In particular, comparison between the modelled and experimental humidification curve, in terms of water content expressed in $\mu g\ m^{-3}$, are presented. Considering the aerosol depositions on insulator surfaces, the comparison was made in terms of water content (mg) normalized against the deposit mass (mg), due to the impossibility of expressing the results in terms of volumetric concentrations.

Notably, the thermodynamic behavior of atmospheric aerosol is closely related to its chemical composition, which can vary significantly depending on the sampling site; therefore, accurate chemical characterization is essential. Hereinafter, results are discussed moving from indoor conditions to outdoor urban and remote sites, till the deposits on insulators at the end.

3.1 Indoor aerosol: a sulfate dominated system case

During the sampling campaigns carried out in 2020–2021 within ROOM 1 and ROOM 2 of a Data Centre (DC) located in the Po Valley, the summer and winter samples were analyzed in IC and AEC.

The average $PM_{2.5}$ concentrations collected on filters for the two rooms for summer and winter were very low due to the high filtering efficiency of the incoming outdoor air; they were:

- ROOM 1-SUMMER: $PM_{2.5} = 1.20 \pm 0.50\ \mu g\ m^{-3}$
- ROOM 2-SUMMER: $PM_{2.5} = 0.79 \pm 0.23\ \mu g\ m^{-3}$
- ROOM 1-WINTER: $PM_{2.5} = 9.58 \pm 0.27\ \mu g\ m^{-3}$
- ROOM 2-WINTER: $PM_{2.5} = 2.33 \pm 0.32\ \mu g\ m^{-3}$

The inorganic composition revealed by the IC analysis, showed in Fig.1, highlighted a different chemical composition between summer and winter samples. In the summer samples sulfates were the major component (71 ± 3 %), followed by ammonium (20 ± 1 %), while nitrates, sodium, calcium, magnesium and potassium account for about 7 ± 3 %. In the winter samples, a

https://doi.org/10.5194/egusphere-2026-3968
Preprint. Discussion started: 17 August 2026

variability between the two rooms was observed: for ROOM 1, the major component is represented by nitrate ion (42 ± 13 %), followed by sulfate (32±14%) and ammonium (21 ± 3 %); for ROOM 2, the sulfate ion (53 ± 10 %) represented the major fraction, followed by ammonium (20 ± 6 %) and nitrate (16 ± 10 %). The reader can see that in ROOM 1 $PM_{2.5}$ concentrations were always higher compared to ROOM 2 due to different outdoor air flow rates (double in ROOM 1 compared to ROOM 2) used in the computing rooms for cooling purposes as detailed in Ferrero et al. (2013); this phenomenon leaves more time for particle–gas phase partitioning in ROOM 2 compared to ROOM 1 enabling a higher loss of NH_4NO_3.

From a modelling interpretation perspective, the nitrate–to–sulfate ratio increased from summertime to wintertime; in particular, for summer samples the average nitrate–to–sulfate ratio was 0.041 ± 0.054, while for winter samples the ratio was 2.83 ± 2.59 for ROOM 1 and 0.59 ± 0.60 for ROOM 2. The DRH of aerosol samples were obtained using the AEC, following the procedure described in Sect. 2.

Given the strong dependence of aerosols thermodynamics on chemical composition, the samples chemically-dominated by sulfates (summer samples and ROOM 2-WINTER) showed a DRH at high level of relative humidity (DRH_s - DRH_e ranges: 63 ± 10 – 80 ± 1 % RH, 67 ± 9 – 80 ± 1 % RH, 65 ± 10 – 81 ± 1 % RH respectively for ROOM 1-SUMMER, ROOM 2-SUMMER and ROOM 2-WINTER), while ROOM 1-WINTER, chemically-dominated by nitrates, showed a DRH at lower values of relative humidity (54 ± 5 – 72 ± 4 % RH) (Martin 2000; Casati et al. 2015).

The comparison between experimental and modelled humidification curves is shown in Fig. 2. The inorganic ionic concentrations identified for the four case studies were used as input for ISORROPIA. The modelled humidification curves reproduce the experimental trend identified in AEC quite well, and the application of ISORROPIA model showed that both maximum hygroscopic growth and DRH values were comparable with the experimental values, in the limit of applicability of the model, which predicts the thermodynamic effect only caused by the inorganic ionic fraction. Considering the starting and the ending point of the deliquescence process, ISORROPIA predicted the DRH_s, and DRH_e with a mean deviation of 0.8±1.3% RH and 2.2±0.8 RH respectively. ISORROPIA performed consistently across the four investigated cases: in summer conditions, DRH_s were reproduced within the experimental variability, whereas DRH_e showed slightly larger departures from observations; in winter, both DRH_s and DRH_e fell within the experimental variability, supporting the robustness of the reliability of the model. All the experimental and modelled DRH values are shown in Table 1.

For winter cases a sulfate–poor and sodium–and–crustal–poor system is identified in ISORROPIA; in these cases, sulfates were neutralized by NH_4^+, Na^+, Ca^{2+}, K^+ and Mg^{2+} with the formation of sulfate salts (e.g. Na_2SO_4, $(NH_4)_2SO_4$, $CaSO_4$, K_2SO_4, $MgSO_4$). Excess ammonium reacted with HNO_3 forming ammonium nitrate. For summer cases, the model identified a sulfate–rich system up to approximately 50 % RH, in which sulfates were only partially neutralized by NH_4^+, Na^+ and crustal species, with the formation of the respective sulfate salts. In this case the balance between sulfates and hydrogen sulfates shifted towards sulfates. The model then involved the same subroutine as in winter cases, moving to a sulfate–poor, sodium–and–crustal–poor system, with the formation of the same sulfate salts as in previous condition.

Under conditions where the contribution of sodium and crustal species, defined by R_2 ratio, is low and the chemical system is dominated by ammonium sulfate or ammonium nitrate, ISORROPIA exhibits stable and predictable behavior. In these regimes,

https://doi.org/10.5194/egusphere-2026-3968
Preprint. Discussion started: 17 August 2026

the model consistently reproduces both the DRH ranges and the associated humidification, confirming that its routines operate reliably in both sulfate–rich and sulfate–poor and sodium–and–crustal–poor conditions.

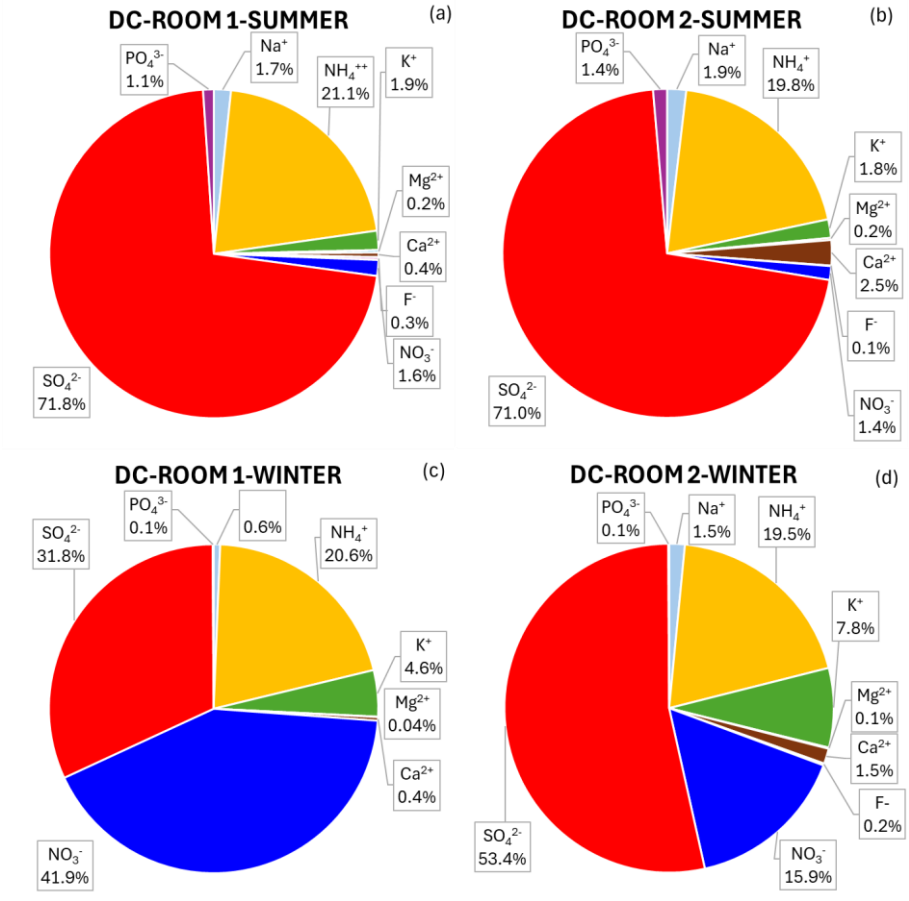

Figure 1: ***Mean chemical inorganic ionic composition (%) for summer and winter samples collected in ROOM 1 (a–c) and ROOM 2 (b–d) of the Data Center (DC).***

https://doi.org/10.5194/egusphere-2026-3968
Preprint. Discussion started: 17 August 2026

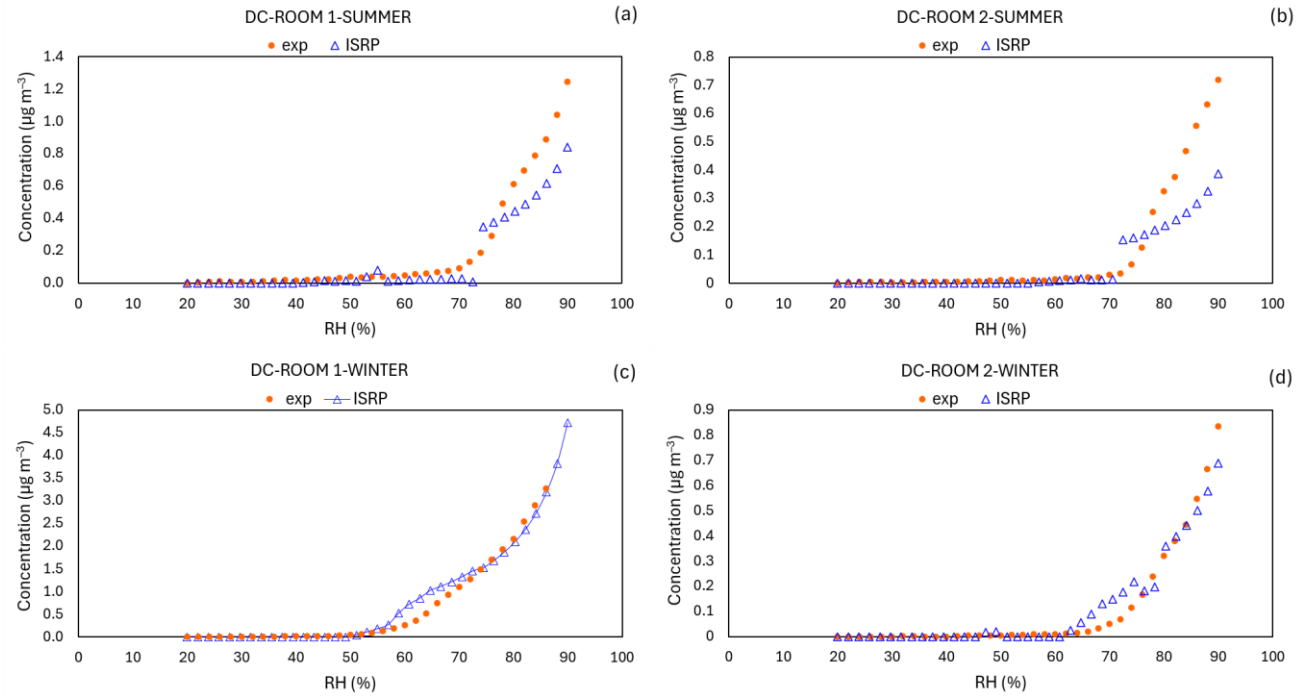

Figure 2: ***Comparison between the experimental and modelled humidification curves for the two sampling sites, ROOM 1 (a-c) and ROOM 2 (b-d) of the Data Center (DC) for summer and winter samples.***

3.2 Outdoor aerosols: urban, extra-urban and marine sites

3.2.1 Urban aerosols and extra-urban aerosols: cases of a nitrate dominated system

Urban aerosol samples were collected in 2022 at the urban background site of the University of Milano-Bicocca (UNIMIB-U9). The campaign involved the collection of 8 aerosol samples ($PM_{2.5}$: 33 ± 10 µg m^{-3}, approximately 50 % explained by inorganic fraction). The samples were analyzed by IC and AEC, identifying, respectively, their inorganic chemical composition and their thermodynamic behavior (Fig.3). The results revealed a nitrate–sulfate–ammonium dominated system, where about a half of the composition (52 ± 7 %) is represented by nitrates, followed by ammonium (22 ± 5 %) and sulfates (15 ± 5 %). Since it was a winter sampling campaign, the average nitrate–to–sulfate ratio was 5.3 ± 3.4, indicating a predominance of nitrates, due to the condensation of ammonium nitrate in the particulate phase favored by the winter low temperatures (Perrone et al. 2010). As the sample was enriched in nitrates, its deliquescence started at low RH values (~40 % RH), since its thermodynamic behavior is mainly driven by the presence of ammonium nitrate (DRH: 60 % RH (Martin 2000)).

Using the inorganic ionic composition revealed by the IC analysis as input for ISORROPIA, the thermodynamic behavior of aerosol was simulated. The comparison between the model output and the experimental results is shown in Fig. 3. The two outputs had a quite good agreement in terms of RH at which humidification starts, only showing a small overestimation of water content by ISORROPIA, with a difference of 28 µg m^{-3} from the experimental reference, probably because ISORROPIA

https://doi.org/10.5194/egusphere-2026-3968
Preprint. Discussion started: 17 August 2026

simulates only the inorganic aerosol phase (Zhang et al. 2020), while the filter samples collected in the atmosphere contain additional components (i.e. organics) that may influence water uptake (Casati et al. 2015; D'Angelo et al. 2017; Ferrero et al. 2020); this is in keeping with the quite monotonic behavior of the experimental curve (Estillore et al. 2017). In fact, in Milan and Po Valley, the biomass burning source can be high in wintertime leading to high sugars content in environmental PM samples (Paglione et al. 2020; D'Angelo et al., 2026).

Despite the difficulty in identifying the experimental DRH values due to the monotonic shape of the curve, the experimental results suggested that the system starts to deliquescence at around 40 % RH, while ISORROPIA predicted the DRH_s at 48 % and the DRH_e at 66 %, resulting, however, consistent with the experimental output. Based on the values of R_1, R_2 and R_3, the model identified a sulfate–poor and sodium–and–crustal–poor system, where the sulfates were neutralized by NH_4^+ and partially by Na^+ and crustal species. The excess of NH_4^+ reacted with HNO_3 and HCl, forming ammonium nitrate and ammonium chloride.

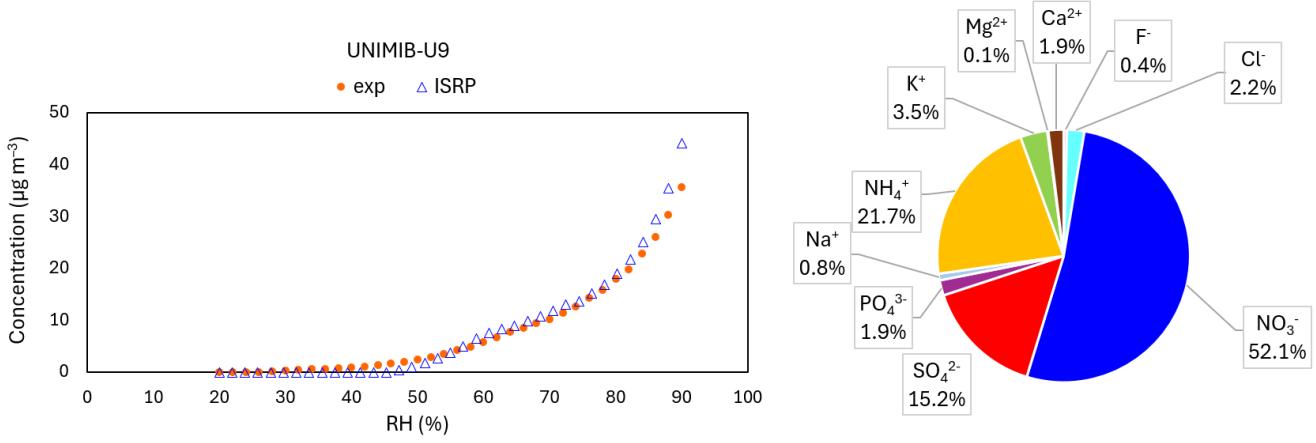

Figure 3: ***Comparison between the experimental and modelled humidification curve of aerosol sampled at the University of Milano-Bicocca sampling site (UNIMIB-U9). Average chemical inorganic ionic composition (%) for samples collected at UNIMIB-U9 sampling site.***

Extra-urban aerosol samples were collected during the 2016–2017 sampling campaign at Milano Malpensa Airport (MXP) in the middle of the green natural park of Ticino Valley; PM_{10} average concentration was 63 ± 51 µg m^{-3}, with approximately 50 % attributed to the inorganic fraction. Samples were analyzed through IC and AEC. Figure 4 illustrates the average relative inorganic chemical composition of the samples. The inorganic aerosol was predominantly made up of nitrate (59 ±10 %), sulfate (14 ± 6 %) and ammonia (13 ± 5 %), with an average nitrate–to–sulfate ratio of 9 ± 14, indicating the prevalence of nitrates over sulfates, largely due to the very large relative uncertainties associated with both species. The content of crustal species ranged from 2.5 % to 20 % depending on the sample. The deliquescence of the system started around 50 % RH, in agreement with its chemical composition mainly composed of nitrates (Casati et al. 2015), as for the urban background case. The subroutine involved in this case identified the same chemical conditions of previous cases (WINTER-DC and UNIMIB-U9). ISORROPIA considered sulfate–poor and sodium–and–crustal–poor conditions, in which all sulfates were neutralized by

https://doi.org/10.5194/egusphere-2026-3968
Preprint. Discussion started: 17 August 2026

ammonium, sodium and crustal species and the excess of ammonia reacted with HNO_3 forming ammonium nitrate. The modelled output based on the average chemical composition showed good agreement with the average experimental curve and both the maximum water uptake and DRH values were comparable (Figure 4). At 90 % RH, ISORROPIA prediction of water content was 171 µg m^{-3}, while the experimental results indicated 120 ± 78 µg m^{-3}, resulting in a difference of 51 µg m^{-3}. As in the previous case (UNIMIB-U9), this discrepancy may be attributed to differences between the modelled and the real aerosol system. The model successfully identified the deliquescence region of the aerosol system, and the predicted values aligned well with experimental data. Experimental DRH_s and DRH_e were 49.2 ± 3.6 % and 64.7 ± 5.8 %, while the corresponding modelled values were 48.0 % and 74.0 %, with a deviation of 1.2 and 9.3 percentage points respectively.

As seen for winter indoor cases, in nitrate–rich and sodium and crustal poor systems, ISORROPIA correctly identifies the threshold at which water absorption begins and subsequent growth, consistently reproducing the observed thermodynamic behavior. In this context, the model shows good reliability, confirming that it operates stably in a sulfate–poor and sodium–and–crustal–poor systems, with differences in the predicted water uptake likely due to the difference between the real and the simulated chemical composition.

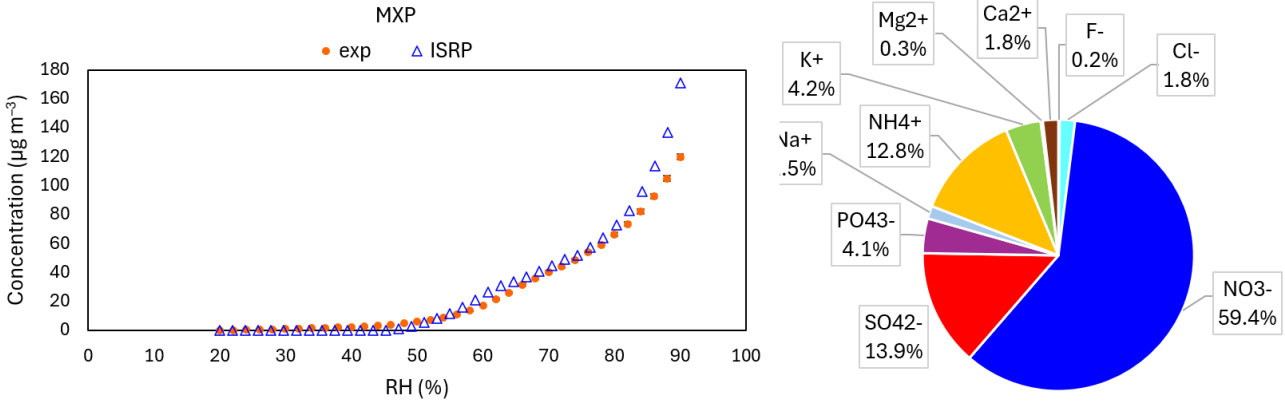

Figure 4: ***Comparison between the experimental and modelled humidification curve of aerosol sampled at Milano Malpensa Airport (MXP). Average chemical inorganic ionic composition (%) of samples.***

3.2.2 Marine aerosols: a case of sodium chloride dominated system

The marine aerosol samples collected during EUREC^{4}A campaign were averagely composed by Cl^- (50 ± 3 %) and Na^+ (28 ± 3 %), which represented about 75 % of the total composition, followed by SO_4^{2-} (11 ± 1 %), NO_3^- (4 ± 3 %), Mg^{2+} (3.3 ± 0.2 %) and K^+ (1.9 ± 0.4 %) (Fig. 5). The samples were analyzed in AEC to identify their DRH values. The identified DRH_s, and DRH_e were 62.0 ± 2.5 %, and 77.8 ± 2.3 % RH respectively. Since the composition is mostly made up of NaCl, the DRH found in AEC agreed with the DRH of NaCl presented in literature (75 ± 1 % RH (Martin 2000)). In this case ISORROPIA showed an irregular trend at low RH, simulating an early hygroscopic growth (20–26 % RH), followed by a crystallization phase in which no water is predicted (28–32 % RH).

https://doi.org/10.5194/egusphere-2026-3968
Preprint. Discussion started: 17 August 2026

Based on the values of R_1, R_2 and R_3 ISORROPIA identified a sulfate–poor, sodium–and–crustal–rich and dust rich system, where the sulfates were fully neutralized by crustal species, forming the respective salts ($CaSO_4$, K_2SO_4 and $MgSO_4$), sodium reacted with HCl and excess of Mg^{2+} reacted with HNO_3 and HCl. The early part of the curve (20–32 % RH) showed an unexpected behavior, with an alternating humidification and crystallization without any thermodynamic explanation. Indeed, between 20 % and 26 % RH, the curve showed immediate growth, as ISORROPIA considers the presence of both solid and liquid phases possible for RH > 20 %. Between 28 % and 32 % RH the curve went to zero because the model used a different subroutine in which only the solid phase is possible. This behavior occurs because each point on the curve represents an independent solution of the ISORROPIA system of equations, with no continuity of the preceding RH step; thus, the model alternating between slightly different computational routines and independent equilibrium states in response to changing RH conditions.

In the case of a marine environment dominated by NaCl, ISORROPIA becomes unstable in reproducing the humidification curve: at low RH it generates variations in the curve that do not appear in the experimental reference and lack a clear thermodynamic explanation. These results highlight that, in sulfate–poor, sodium–and–crustal–rich and dust rich systems, the model may show limitations in representing hygroscopic evolution, which could reflect specific sensitivities of ISORROPIA under these chemical conditions.

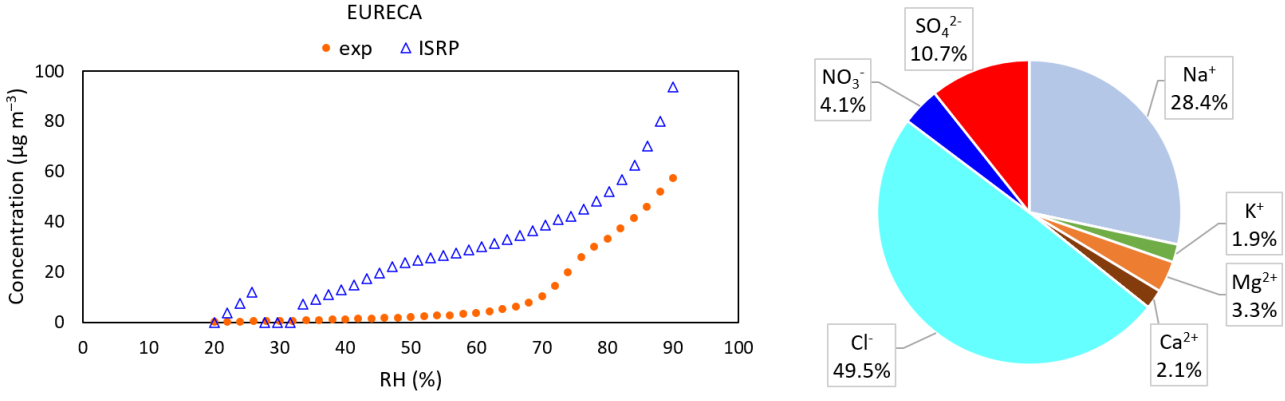

Figure 5: ***Comparison between the experimental and modelled humidification curve of aerosol sampled during EUREC⁴A campaign. Average chemical inorganic ionic composition (%) of samples.***

3.3 Deposit of aerosol collected on the Italian insulator surfaces: cases with sodium and crustal influenced system

The deposition of atmospheric aerosol on overhead power line insulators can pose a potential flashover hazard, which may compromise the performance of power grid (Mohammadnabi and Rahmani 2021). To investigate this issue, a sampling campaign focused on chemically characterizing the aerosol deposits was carried out in 2016–2018 across the three Italian macro-regions (MRs; see section 2.1) Ionic insulator contamination was found to be higher in MR1 (Islands: 82.54 ± 13.92 µg cm^{-2}) and decrease towards MR2 (Tyrrhenian region: 26.74 ± 2.60 µg cm^{-2}) and MR3 (Adriatic and inland region: 10.65 ± 1.07 µg cm^{-2}). As shown in Fig. 6, the ionic inorganic composition varied between the MRs. In particular,

https://doi.org/10.5194/egusphere-2026-3968
Preprint. Discussion started: 17 August 2026

MR1 is characterized by a great amount of chloride (26 ± 11 %), followed by sulfate (24 ± 14 %), calcium (19 ± 9 %) and sodium (16 ± 5 %); MR2 is mainly characterized by chloride (27 ± 11 %), nitrate (18 ± 14 %), sodium (18 ± 5 %), calcium (17 ± 9 %) and sulfate (14 ± 7 %); MR3 is mostly made up of nitrate (23 ± 17 %), calcium (20 ± 10 %), chloride (19 ± 12 %), sodium (17 ± 7 %) and sulfate (12±6%). Due to the high variability in the data, the standard deviation is high, reflecting the large heterogeneity in the relative ion composition across the MRs. Considering the relative ion composition, while the contribution of sulfate followed the same trend of the total contamination, decreasing from MR1 to MR3, nitrate's contribution exhibits the opposite trend (MR3>MR2>MR1; see Gini et al. (2023)); indeed, the nitrate–to–sulfate ratio went from 0.34 ± 0.63 in MR1, 2.03 ± 3.02 in MR2 and 3.43 ± 4.47 in MR3, affecting the DRH of the MRs.

To study the thermodynamic behavior of the collected aerosol samples, following the methodology described in Sect. 2.4, synthetic aerosol with a chemical composition similar to that measured by IC for each MR was generated in laboratory and deposited on Teflon filters. Figure 6 shows the average inorganic chemical composition of each MR determined from the samples, while the synthetic chemical composition used to perform the analyses in AEC is presented in the supplementary materials, Fig. S6. The filters were analyzed in AEC, and the DRH of each MR was obtained. Since this study focused on aerosol depositions on a surface rather than atmospheric aerosol, the comparison between the experimental and modelled curves is based on the mass of water content normalized to the deposition mass, rather than air concentrations; for the same reason, ISORROPIA inputs were defined using the mass (mg) of each measured ion.

To execute the simulations in ISORROPIA, shown in Fig. 6, the ions content of the collected samples was used; in the supplementary materials (Fig. S7) the simulation using the content of the synthetic aerosol samples generated for the AEC analyses are shown.

ISORROPIA simulations revealed irregular trends in all three cases (Fig. 6). Based on the values of R_1, R_2 and R_3, ISORROPIA identified a sulfate–poor, sodium–and–crustal rich and dust–poor system for DEP-MR1, and a sulfate poor, sodium–and–crustal rich and dust–rich system for DEP-MR2 and DEP-MR3. Particularly, DEP-MR1 showed a drop in the curve to zero between 62–66% RH, due to the shift in the subroutine used by the model, which provides different conditions than the previous one. A similar scenario is shown in DEP-MR3, where the curve drops back to zero between 30–32 % RH. In all cases, the simulated humidification curve started immediately to grow, differing from the experimental references.

https://doi.org/10.5194/egusphere-2026-3968
Preprint. Discussion started: 17 August 2026

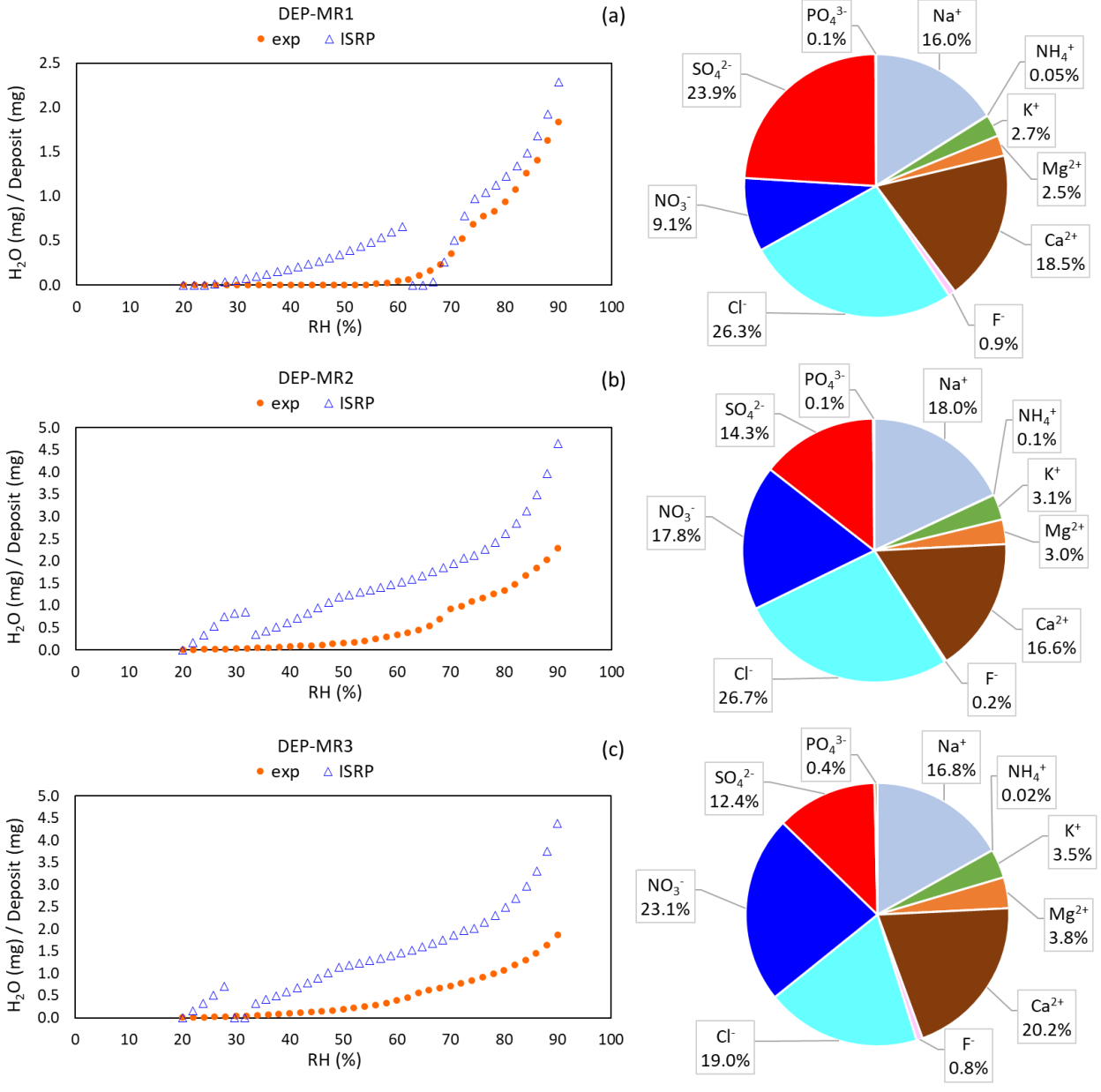

Figure 6: ***Comparison between experimental and modelled humidification curve of MR1 (a), MR2 (b), MR3 (c) together with the relative ionic composition (% mass) identified for each macro-region during the 2016–2018 campaign.***

When ISORROPIA was applied to a sulfate–nitrate–ammonium dominated system it provided outputs that were consistent with experimental results. This agreement is particularly evident in the samples collected in indoor environment, as well as at urban (UNIMIB – U9) and extra-urban (MXP) sites. In these cases, the model successfully captured the thermodynamic behavior of the aerosol system, accurately describing its phase transitions. However, when ISORROPIA was applied to a system characterized by low ammonium content, where sodium, calcium, potassium and magnesium act as the main

https://doi.org/10.5194/egusphere-2026-3968
Preprint. Discussion started: 17 August 2026

counterions, unexpected trends emerged. As observed in cases such as EUREC^{4}A, DEP-M1, DEP-MR2 and DEP-MR3, which work in sulfate–poor and sodium–and–crustal rich conditions, the model exhibited anomalous trends, including an irregular alternation between deliquescence and crystallization phases, without a clear thermodynamic explanation. These behaviors raised concerns regarding the applicability of ISORROPIA to such systems and suggested the need for a deeper investigation.

3.4 Synthetic aerosol: cases with controlled chemical composition

To address the aforementioned concerns (Sect. 3.3), a systematic study of ISORROPIA's behavior was conducted, starting with simulations of pure salts to evaluate its response under controlled conditions (see Sect. 2.4). The results highlighted notable inconsistencies depending on the salt under consideration. For some salts, such as sodium chloride and sodium nitrate (supplementary materials, Fig. S8), the model's output was consistent with the well-documented hygroscopic properties of the compound (Martin 2000); while for other salts, such as magnesium chloride and calcium nitrate (Fig. 7), ISORROPIA showed unexpected behaviors, including an irregular alternation between growing and decreasing phases. To simulate the thermodynamic behavior of magnesium chloride and calcium nitrate, based on the values of R_1, R_2 and R_3, the model selected a sulfate–poor, sodium–and–crustal–rich and dust–rich regime. As in EUREC^{4}A and DEP-MR3, the curves showed immediate growth, as ISORROPIA considers the presence of both solid and liquid phases possible at RH > 20 %. For magnesium chloride, the model shifted to a subroutine that considers only the presence of solid phase; for calcium nitrate, at 28 % the liquid phase is reset, and the model recalculates growth using a different subroutine that considers the presence of both solid and liquid phases possible. To further explore these discrepancies, the thermodynamic behavior of these salts was experimentally analyzed using the AEC to establish an experimental reference to compare the model's outputs with. The DRH values obtained from AEC experiments were in good agreement with literature (Tang and Fung 1997; Al-Abadleh et al. 2003; A. Wang et al. 2009; Heinz et al. 2016), providing a robust basis for comparison with ISORROPIA's outputs.

Even with synthetic aerosol, when ISORROPIA was applied to a system without ammonium and only with magnesium and calcium an unexpected trend emerged (Fig. 7) exhibiting an irregular alternation between deliquescence and crystallization phases, without a clear thermodynamic explanation. These behaviors brought to the need for an improvement of the model which is presented in Sect. 3.5.

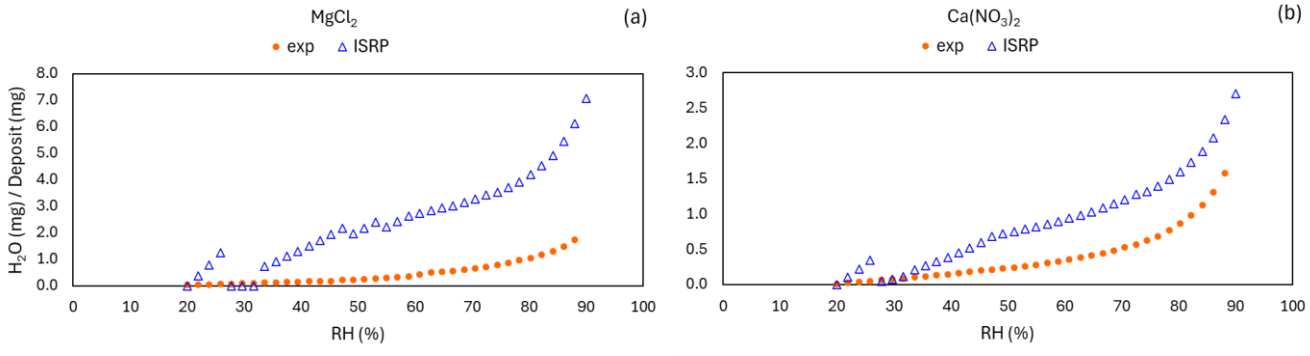

Figure 7: ***Comparison between experimental and modelled humidification curve of magnesium chloride (a) and calcium nitrate (b).***

https://doi.org/10.5194/egusphere-2026-3968
Preprint. Discussion started: 17 August 2026

3.5 ISORROPIA improvement

In light of the aforementioned findings, a series of coding refinements were proposed to improve the model's performance in ammonium–poor and crustal–species–enriched systems. These refinements (detailed in supplementary material) include improved handling of specific ionic species, adjustments to the management of ionic activity and updates to the subroutine selection criteria. Overall, these improvements aim to increase ISORROPIA's predictive accuracy and ensure its applicability in a wider range of conditions.

The revised version of ISORROPIA, named 2.1*, was subsequently applied to the previously identified anomalous cases: EUREC^{4}A, DEP-MR1, DEP-MR2, DEP-MR3. The coding refinements improved the model's applicability to ammonium–poor and crustal–species–rich systems, leading to more consistent and physically interpretable thermodynamic behavior. As an example, Fig. 8 shows the simulations for DEP-MR1 and EUREC^{4}A, where the model output exhibits a more realistic phase transition, with better agreement with experimental reference especially for DEP-MR1 where the agreement was excellent showing that both maximum hygroscopic growth and DRH values were comparable to experimental ones, while for EURAC^{4}A the model still overestimates the water content as well as the starting of the deliquescence region. Revised ISORROPIA predicted a deliquescence region between 60.0 % and 74.0 % RH, in agreement with the experimental deliquescence region (63.3 ± 2.3 % and 74.7 ± 2.3 % RH). For the EUREC^{4}A case, the revised ISORROPIA showed a improvement compared to the standard ISORROPIA. Although it was not fully aligned with experimental observations, it avoided predicting a complete depletion of water content and instead simulated a slight decrease between 30% and 34% RH. However, DRH values remain inconsistent with measurements: revised ISORROPIA predicted the start of the deliquescence process at 28 % RH and its end at 50 % RH, while experimental output place the deliquescence region between 62±2.5% and 77.8 ± 2.3 % RH (Table 1). Additional simulation results for DEP-MR2 and DEP-MR3 are provided in the supplementary materials (Fig S9).

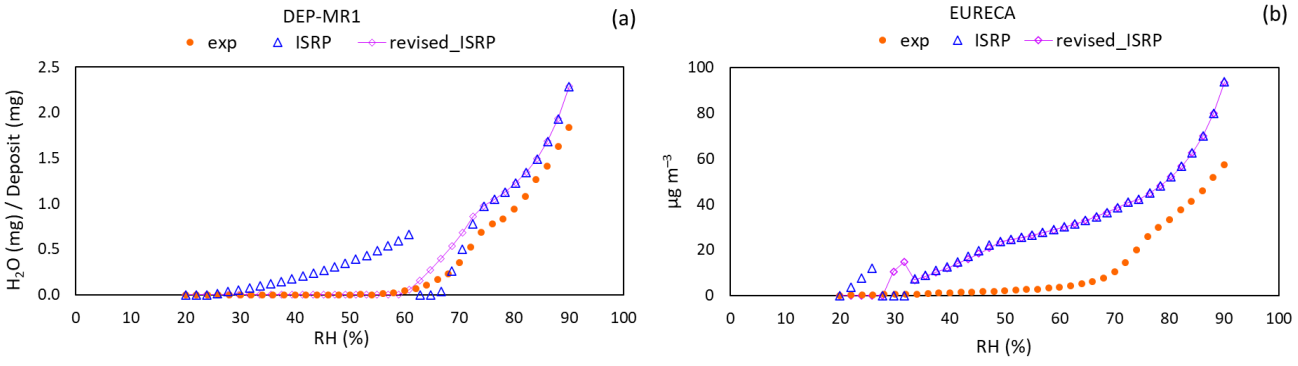

Figure 8: ***Comparison between experimental (orange) and modelled humidification curves with standard version (blue) and revised version (pink) of ISORROPIA: (a) DEP-MR1; (b) EURECA.***

https://doi.org/10.5194/egusphere-2026-3968
Preprint. Discussion started: 17 August 2026

Table 1: ***Experimental and modelled DRH_s and DRH_e values of all case studies. EURECA, DEP-MR1, DEP-MR2, DEP-MR3 were simulated with standard and revised version of ISORROPIA. The asterisk (*) indicates the value is difficult to determine due to the shape of the curve.***

Case study	Parameter	Phase Transitions (RH %)	
		DRH_s	DRH_e
ROOM 1-SUMMER	Exp ± dev.st	63.4 ± 10.1	79.7 ± 1.4
	ISRP	70	76
ROOM 1-WINTER	Exp ± dev.st	54.3 ± 5.5	72 ± 3.9
	ISRP	50	74
ROOM 2-SUMMER	Exp ± dev.st	66.6 ± 8.8	79.7 ± 1.4
	ISRP	70	74
ROOM 2-WINTER	Exp ± dev.st	64.5 ± 10.3	81.3 ± 1.5
	ISRP	62	80
UNIMIB-U9	Exp ± dev.st	~40*	*
	ISRP	48	66
MXP	Exp ± dev.st	49.2 ± 3.6	64.7 ± 5.8
	ISRP	48	74
EURECA	Exp ± dev.st	62.0 ± 2.5	77.8 ± 2.3
	ISRP	*	*
	Revised ISRP	28	50
DEP-MR1	Exp ± dev.st	63.3 ± 2.3	74.7 ± 2.3
	ISRP	*	*
	Revised ISRP	60	74
DEP-MR2	Exp ± dev.st	61.3 ± 1.2	70 ± 0.1
	ISRP	*	*
	Revised ISRP	34	50
DEP-MR3	Exp ± dev.st	55.3 ± 2.3	66.7 ± 1.2
	ISRP	*	*
	Revised ISRP	28	50

https://doi.org/10.5194/egusphere-2026-3968
Preprint. Discussion started: 17 August 2026

4. Conclusions

The study evaluated the performance of the thermodynamic model ISORROPIA 2.1 across a wide range of aerosol systems, including indoor, urban, extra-urban, marine environments, and surface deposits on electrical insulators.

The methodological framework adopted in this study, comprising multi-context aerosol sampling, controlled thermodynamic characterization in the Aerosol Exposure Chamber (AEC), and subsequent modelling with ISORROPIA 2.1, proved essential for establishing a coherent and reproducible basis for model evaluation.

The results indicate that ISORROPIA 2.1 performs well when applied to sulfate–nitrate–ammonium dominated aerosols, successfully capturing deliquescence, DRH values and water uptake, in agreement with experimental data, with discrepancies due to the differences between real and simulated system, probably attributable to the presence of organic aerosol components in the experimental samples. However, when applied to ammonium–poor systems enriched in alkali and alkaline–earth metals (Na^+, K^+, Mg^{2+}, Ca^{2+}), the model exhibited inconsistent and thermodynamically unrealistic behaviors, including irregular phase transitions. These anomalies were further confirmed by simulating individual salt systems, such as magnesium chloride and calcium nitrate, highlighting specific challenges in representing crustal–rich aerosol. To address these limitations, targeted refinements were introduced to the ISORROPIA 2.1 code, improving its predictive reliability and physical interpretability of the humidification curves for ammonium–poor and crustal–rich systems, although residual discrepancies persist in specific cases (e.g., EUREC^{4}A marine aerosol samples). In particular, simulations of insulator-deposit samples showed a marked improvement, confirming the effectiveness of the updates.

A notable strength of the methodological approach concerns the treatment of deposited aerosols on power-line insulators. Unlike atmospheric PM samples, these materials required the laboratory generation of synthetic aerosol to reproduce real contamination patterns under controlled conditions. The agreement between the modelled behavior of synthetic and ambient-derived mixtures confirms the robustness of the methodology and its suitability for applications beyond conventional atmospheric aerosol studies.

Overall, the results demonstrate that the integrated framework is a reliable and internally consistent approach for investigating aerosol phase transitions across different chemical regimes. However, it is worth mentioning that while ISORROPIA 2.1 remains highly reliable for ammonium–rich systems, its application to crustal–rich aerosol requires careful consideration and, in some cases, adjusted model formulations.

Future developments should aim to resolve the remaining inconsistencies between experimental observations and model predictions in crustal–rich and marine aerosol systems. Further refinement of activity coefficient treatments, improved subroutine selection criteria, and the expansion of experimental datasets under controlled chemical conditions will be essential to enhance the representation of complex inorganic aerosols in thermodynamic equilibrium models.

https://doi.org/10.5194/egusphere-2026-3968
Preprint. Discussion started: 17 August 2026

Code, data, or code and data availability

The code of ISORROPIA 2.1* used in this study has not been deposited in a public repository due to restrictions on its public redistribution from RSE. The implementation used for the simulations is available from the corresponding author upon reasonable request.

Supplement

The supplementary material includes additional figures, methodological details, synthetic aerosol compositions, additional ISORROPIA 2.1 simulations and details of its improvement.

Author contributions

Conceptualization: IG, LF, GP, AB; methodology: IG, GP, LF; data curation: IG, LF; formal analysis: IG, MB, GP, AB, LF; investigation: AMC, AD, LG, NL; software: IG, GP, AB; writing – original draft: IG; writing – review and editing: IG, MB, GP, AB, LF; supervision: GP, LF, EGB.

Competing interests

The authors declare that they have no conflict of interest.

Acknowledgements

This work has been financed by the Research Fund for the Italian Electrical System under the Three–Year Research Plan 2025–2027 (MASE, Decree n.388 of November 6th, 2024) in compliance with the Decree of April 12th, 2024".

This work is an output of the GEMMA Center in the framework of project MUR TECLA "Dipartimenti di Eccellenza 2023–2027".

Financial support

This work has been financed by the Research Fund for the Italian Electrical System under the Three–Year Research Plan 2025–2027 (MASE, Decree n.388 of November 6th, 2024) in compliance with the Decree of April 12th, 2024".

https://doi.org/10.5194/egusphere-2026-3968
Preprint. Discussion started: 17 August 2026

This work is an output of the GEMMA Center in the framework of project MUR TECLA "Dipartimenti di Eccellenza 2023–2027".

References

Al-Abadleh, Hind A., B. J. Krueger, J. L. Ross, and V. H. Grassian. 2003. 'Phase Transitions in Calcium Nitrate Thin Films'. *Chem. Commun.*, no. 22: 2796–97. https://doi.org/10.1039/B308632A.

Ansari, Asif S., and Spyros N. Pandis. 1999. 'An Analysis of Four Models Predicting the Partitioning of Semivolatile Inorganic Aerosol Components'. *Aerosol Science and Technology* 31 (2–3): 129–53. https://doi.org/10.1080/027868299304200.

Berman, Bryan C., Bryan E. Cummings, Anita M. Avery, Peter F. DeCarlo, Shannon L. Capps, and Michael S. Waring. 2022. 'Simulating Indoor Inorganic Aerosols of Outdoor Origin with the Inorganic Aerosol Thermodynamic Equilibrium Model ISORROPIA'. *Indoor Air* 32 (7). https://doi.org/10.1111/ina.13075.

Calvin, Katherine, Dipak Dasgupta, Gerhard Krinner, et al. 2023. *IPCC, 2023: Climate Change 2023: Synthesis Report. Contribution of Working Groups I, II and III to the Sixth Assessment Report of the Intergovernmental Panel on Climate Change [Core Writing Team, H. Lee and J. Romero (Eds.)]. IPCC, Geneva, Switzerland.* First. Edited by Paola Arias, Mercedes Bustamante, Ismail Elgizouli, et al. With Hoesung Lee. Intergovernmental Panel on Climate Change (IPCC). https://doi.org/10.59327/IPCC/AR6-9789291691647.

Casati, Marco, Grazia Rovelli, Luca D'Angelo, et al. 2015. 'Experimental Measurements of Particulate Matter Deliquescence and Crystallization Relative Humidity: Application in Heritage Climatology'. *Aerosol and Air Quality Research* 15: 399–409. https://doi.org/10.4209/aaqr.2014.11.0289.

Cheng, Mingkai, Liang Chen, Ziyue Meng, et al. 2025. 'The Influence of Alkali Metals on PM10 Emission Characteristics during Waste Combustion'. *Journal of Physics: Conference Series* 3159 (1): 012001. https://doi.org/10.1088/1742-6596/3159/1/012001.

Cheng, Wei, Jianfeng Chen, Wei Yang, et al. 2024. 'Effect of Sludge-Based Additive on Particulate Matter Emission during the Combustion of Agricultural Biomass Pellet'. *Energy* 313 (December): 133769. https://doi.org/10.1016/j.energy.2024.133769.

Cheung, Hing Cho, Charles Chung-Kuang Chou, Celine Siu Lan Lee, Wei-Chen Kuo, and Shuenn-Chin Chang. 2020. 'Hygroscopic Properties and Cloud Condensation Nuclei Activity of Atmospheric Aerosols under the Influences of Asian Continental Outflow and New Particle Formation at a Coastal Site in Eastern Asia'. *Atmospheric Chemistry and Physics* 20 (10): 5911–22. https://doi.org/10.5194/acp-20-5911-2020.

Chianese, Elena, Giuseppina Tirimberio, Adelaide Dinoi, et al. 2022. 'Particulate Matter Ionic and Elemental Composition during the Winter Season: A Comparative Study among Rural, Urban and Remote Sites in Southern Italy'. *Atmosphere* 13 (2): 356. https://doi.org/10.3390/atmos13020356.

Chithra, V. S., and S. M. Shiva Nagendra. 2013. 'Chemical and Morphological Characteristics of Indoor and Outdoor Particulate Matter in an Urban Environment'. *Atmospheric Environment* 77 (October): 579–87. https://doi.org/10.1016/j.atmosenv.2013.05.044.

https://doi.org/10.5194/egusphere-2026-3968
Preprint. Discussion started: 17 August 2026

Choi, Man Yee, and Chak K. Chan. 2002. 'The Effects of Organic Species on the Hygroscopic Behaviors of Inorganic Aerosols'. *Environmental Science & Technology* 36 (11): 2422–28. https://doi.org/10.1021/es0113293.

Clegg, Simon L., Kenneth S. Pitzer, and Peter Brimblecombe. 1992. 'Thermodynamics of Multicomponent, Miscible, Ionic Solutions. Mixtures Including Unsymmetrical Electrolytes'. *The Journal of Physical Chemistry* 96 (23): 9470–79. https://doi.org/10.1021/j100202a074.

Couvidat, Florian, Bertrand Bessagnet, Marta Garcia-Vivanco, Elsa Real, Laurent Menut, and Augustin Colette. 2018. 'Development of an Inorganic and Organic Aerosol Model (CHIMERE 2017 β v1.0): Seasonal and Spatial Evaluation over Europe'. *Geoscientific Model Development* 11 (1): 165–94. https://doi.org/10.5194/gmd-11-165-2018.

Dalkhsuren, Davaajav, Kazunori Iwabuchi, Takanori Itoh, et al. 2023. 'Effects of Ash Composition and Combustion Temperature on Reduced Particulate Matter Emission by Biomass Carbonization'. *BioEnergy Research* 16 (3): 1629–38. https://doi.org/10.1007/s12155-022-10526-x.

D'Angelo, Luca, Grazia Rovelli, Marco Casati, et al. 2016. 'Seasonal Behavior of PM2.5 Deliquescence, Crystallization, and Hygroscopic Growth in the Po Valley (Milan): Implications for Remote Sensing Applications'. *Atmospheric Research* 176–177 (July): 87–95. https://doi.org/10.1016/j.atmosres.2016.02.011.

D'Angelo, Luca, V. Verdingovas, Luca Ferrero, Ezio Bolzacchini, and R. Ambat. 2017. 'On the Effects of Atmospheric Particles Contamination and Humidity on Tin Corrosion'. *IEEE Transactions on Device and Materials Reliability* 17 (4): 746–57. https://doi.org/10.1109/TDMR.2017.2771505.

Estillore, Armando D., Holly S. Morris, Victor W. Or, et al. 2017. 'Linking Hygroscopicity and the Surface Microstructure of Model Inorganic Salts, Simple and Complex Carbohydrates, and Authentic Sea Spray Aerosol Particles'. *Physical Chemistry Chemical Physics* 19: 21101–11. https://doi.org/10.1039/C7CP04051B.

Ferrero, Luca, Alessandra Bigogno, Amedeo M. Cefalì, et al. 2020. 'On the Synergy between Elemental Carbon and Inorganic Ions in the Determination of the Electrical Conductance Properties of Deposited Aerosols: Implications for Energy Applications'. *Applied Sciences* 10 (16): 5559. https://doi.org/10.3390/app10165559.

Ferrero, Luca, Marco Casati, Lara Nobili, et al. 2018. 'Chemically and Size-Resolved Particulate Matter Dry Deposition on Stone and Surrogate Surfaces inside and Outside the Low Emission Zone of Milan: Application of a Newly Developed "Deposition Box"'. *Environmental Science and Pollution Research* 25 (10): 9402–15. https://doi.org/10.1007/s11356-018-1220-2.

Ferrero, Luca, Luca D'Angelo, Grazia Rovelli, et al. 2015. 'Determination of Aerosol Deliquescence and Crystallization Relative Humidity for Energy Saving in Free-Cooled Data Centers'. *International Journal of Environmental Science and Technology* 12 (9): 2777–90. https://doi.org/10.1007/s13762-014-0680-2.

Ferrero, Luca, Asta Gregorič, Griša Močnik, et al. 2021. 'The Impact of Cloudiness and Cloud Type on the Atmospheric Heating Rate of Black and Brown Carbon in the Po Valley'. *Atmospheric Chemistry and Physics* 21: 4869–97. https://doi.org/10.5194/acp-21-4869-2021.

Ferrero, Luca, Giorgia Sangiorgi, Barbara Ferrini, et al. 2013. 'Aerosol Corrosion Prevention and Energy-Saving Strategies in the Design of Green Data Centers'. *Environmental Science*.

Fountoukis, C., and A. Nenes. 2007. 'ISORROPIA II: A Computationally Efficient Thermodynamic Equilibrium Model for K^+ –Ca^{2+} –Mg^{2+} –NH_4^+ –Na^+ –SO_4^{2-} –NO_3^- –Cl^- –H_2O Aerosols'. *Atmospheric Chemistry and Physics* 7 (17): 4639–59. https://doi.org/10.5194/acp-7-4639-2007.

https://doi.org/10.5194/egusphere-2026-3968
Preprint. Discussion started: 17 August 2026

Fuzzi, S., U. Baltensperger, K. Carslaw, et al. 2015. 'Particulate Matter, Air Quality and Climate: Lessons Learned and Future Needs'. *Atmospheric Chemistry and Physics* 15 (14): 8217–99. https://doi.org/10.5194/acp-15-8217-2015.

Gini, Irene, Alessandra Balzarini, Guido Pirovano, et al. 2023. 'On the Chemical Composition and Hygroscopicity of Aerosols Deposited on the Insulators of Italian Power Lines'. *Applied Sciences* 13 (23): 12788. https://doi.org/10.3390/app132312788.

Grell, Georg, Steven Peckham, Rainer Schmitz, et al. 2005. *Fully Coupled 'Online' Chemistry within the WRF Model*. https://doi.org/https://doi.org/10.1016/j.atmosenv.2005.04.027.

Guo, Liya, Wenjun Gu, Chao Peng, et al. 2019. 'A Comprehensive Study of Hygroscopic Properties of Calcium- and Magnesium-Containing Salts: Implication for Hygroscopicity of Mineral Dust and Sea Salt Aerosols'. *Atmospheric Chemistry and Physics* 19 (4): 2115–33. https://doi.org/10.5194/acp-19-2115-2019.

Gupta, D., H. J. Eom, H. R. Cho, and C. U. Ro. 2015. 'Hygroscopic Behavior of NaCl–$MgCl_2$ Mixture Particles as Nascent Sea-Spray Aerosol Surrogates and Observation of Efflorescence during Humidification'. *Atmospheric Chemistry and Physics* 15 (19): 11273–90. https://doi.org/10.5194/acp-15-11273-2015.

Haddrell, Allen E., David Lewis, Tanya Church, Reinhard Vehring, Darragh Murnane, and Jonathan P. Reid. 2017. 'Pulmonary Aerosol Delivery and the Importance of Growth Dynamics'. *Therapeutic Delivery* 8 (12): 1051–61. https://doi.org/10.4155/tde-2017-0093.

Heintzenberg, Jost. 1989. 'Fine Particles in the Global Troposphere A Review'. *Tellus B* 41B (2): 149–60. https://doi.org/10.1111/j.1600-0889.1989.tb00132.x.

Heinz, Jacob, Dirk Schulze-Makuch, and Samuel P. Kounaves. 2016. 'Deliquescence-induced Wetting and RSL-like Darkening of a Mars Analogue Soil Containing Various Perchlorate and Chloride Salts'. *Geophysical Research Letters* 43 (10): 4880–84. https://doi.org/10.1002/2016GL068919.

Jabłońska, Mariola, Janusz Janeczek, and Beata Smieja-Król. 2021. 'The Impact of Ambient Atmospheric Mineral-Dust Particles on the Calcification of Lungs'. *Minerals* 11 (2): 125. https://doi.org/10.3390/min11020125.

Kakavas, Stylianos, Spyros N. Pandis, and Athanasios Nenes. 2022. 'ISORROPIA-Lite: A Comprehensive Atmospheric Aerosol Thermodynamics Module for Earth System Models'. *Tellus B: Chemical and Physical Meteorology* 74 (1): 1. https://doi.org/10.16993/tellusb.33.

Kelly, Paul, Sonja Kahlmeier, Thomas Götschi, et al. 2014. 'Systematic Review and Meta-Analysis of Reduction in All-Cause Mortality from Walking and Cycling and Shape of Dose Response Relationship'. *International Journal of Behavioral Nutrition and Physical Activity* 11 (1): 132. https://doi.org/10.1186/s12966-014-0132-x.

Kim, Yong Pyo, and John H. Seinfeld. 1995. 'Atmospheric Gas–Aerosol Equilibrium: III. Thermodynamics of Crustal Elements Ca^{2+} , K^{+} , and Mg^{2+}'. *Aerosol Science and Technology* 22 (1): 93–110. https://doi.org/10.1080/02786829408959730.

Kim, Yong Pyo, John H. Seinfeld, and Pradeep Saxena. 1993a. 'Atmospheric Gas-Aerosol Equilibrium I. Thermodynamic Model'. *Aerosol Science and Technology* 19 (2): 157–81. https://doi.org/10.1080/02786829308959628.

Kim, Yong Pyo, John H. Seinfeld, and Pradeep Saxena. 1993b. 'Atmospheric Gas-Aerosol Equilibrium II. Analysis of Common Approximations and Activity Coefficient Calculation Methods'. *Aerosol Science and Technology* 19 (2): 182–98. https://doi.org/10.1080/02786829308959629.

https://doi.org/10.5194/egusphere-2026-3968
Preprint. Discussion started: 17 August 2026

Lei, Yu, Yanqing Niu, Wen'an Ma, et al. 2022. 'Study on the Formation of Ultrafine Particulate Matter (PM) during Char Combustion in a Wet Oxy-Combustion Atmosphere'. *International Journal of Greenhouse Gas Control* 115 (March): 103617. https://doi.org/10.1016/j.ijggc.2022.103617.

Litvak, Andres, Ashok J. Gadgil, and W. J. Fisk. 2000. 'Hygroscopic Fine Mode Particle Deposition on Electronic Circuitsand Resulting Degradation of Circuit Performance: An ExperimentalStudy'. *Indoor Air* 10: 47–56.

Liu, Li, Ye Kuang, Miaomiao Zhai, et al. 2022. 'Strong Light Scattering of Highly Oxygenated Organic Aerosols Impacts Significantly on Visibility Degradation'. *Atmospheric Chemistry and Physics* 22 (11): 7713–26. https://doi.org/10.5194/acp-22-7713-2022.

Makar, P. A., V. S. Bouchet, and A. Nenes. 2003. 'Inorganic Chemistry Calculations Using HETV—a Vectorized Solver for the SO42−–NO3−–NH4+ System Based on the ISORROPIA Algorithms'. *Atmospheric Environment* 37 (16): 2279–94. https://doi.org/10.1016/S1352-2310(03)00074-8.

Martin, Scot T. 2000. 'Phase Transitions of Aqueous Atmospheric Particles'. *Chemical Reviews* 100 (9): 3403–54. https://doi.org/10.1021/cr990034t.

Martin, Scot T., Julie C. Schlenker, Adam Malinowski, Hui-Ming Hung, and Yinon Rudich. 2003. 'Crystallization of Atmospheric Sulfate-nitrate-ammonium Particles'. *Geophysical Research Letters* 30 (21): 2003GL017930. https://doi.org/10.1029/2003GL017930.

Meng, Zhaoyue, John H. Seinfeld, Pradeep Saxena, and Yong Pyo Kim. 1995. 'Atmospheric Gas-Aerosol Equilibrium: IV. Thermodynamics of Carbonates'. *Aerosol Science and Technology* 23 (2): 131–54. https://doi.org/10.1080/02786829508965300.

Metzger, Swen, Frank Dentener, Maarten Krol, Ad Jeuken, and Jos Lelieveld. 2002. 'Gas/Aerosol Partitioning 2. Global Modeling Results'. *Journal of Geophysical Research: Atmospheres* 107 (D16). https://doi.org/10.1029/2001JD001103.

Metzger, Swen, Frank Dentener, Spyros Pandis, and Jos Lelieveld. 2002. 'Gas/Aerosol Partitioning: 1. A Computationally Efficient Model'. *Journal of Geophysical Research: Atmospheres* 107 (D16). https://doi.org/10.1029/2001JD001102.

Metzger, Swen, N. Mihalopoulos, and J. Lelieveld. 2006. 'Importance of Mineral Cations and Organics in Gas-Aerosol Partitioning of Reactive Nitrogen Compounds: Case Study Based on MINOS Results'. *Atmos. Chem. Phys.*

Mohammadnabi, S., and Kh. Rahmani. 2021. 'Influence of Humidity and Contamination on the Leakage Current of 230-kV Composite Insulator'. *Electric Power Systems Research* 194 (May): 107083. https://doi.org/10.1016/j.epsr.2021.107083.

Nenes, Athanasios, Spyros N. Pandis, and Christodoulos Pilinis. 1998. 'ISORROPIA: A New Thermodynamic Equilibrium Model for Multiphase Multicomponent Inorganic Aerosols'. *Aquatic Geochemistry* 4 (1): 123–52. https://doi.org/https://doi.org/10.1023/A:1009604003981.

Nenes, Athanasios, Spyros N. Pandis, and Christodoulos Pilinis. 1999. 'Continued Development and Testing of a New Thermodynamic Aerosol Module for Urban and Regional Air Quality Models'. *Atmospheric Environment* 33 (10): 1553–60. https://doi.org/10.1016/S1352-2310(98)00352-5.

https://doi.org/10.5194/egusphere-2026-3968
Preprint. Discussion started: 17 August 2026

Neuberger, Almuth, Stefano Decesari, Andreas Aktypis, et al. 2025. 'From Molecules to Droplets: The Fog and Aerosol Interaction Research Italy (FAIRARI) 2021/22 Campaign'. *Bulletin of the American Meteorological Society* 106 (1): E23–50. https://doi.org/10.1175/BAMS-D-23-0166.1.

Norman, Olivia G., Colette L. Heald, Solomon Bililign, et al. 2025. 'Exploring the Processes Controlling Secondary Inorganic Aerosol: Evaluating the Global GEOS-Chem Simulation Using a Suite of Aircraft Campaigns'. *Atmospheric Chemistry and Physics* 25 (2): 771–95. https://doi.org/10.5194/acp-25-771-2025.

Paglione, Marco, Stefania Gilardoni, Matteo Rinaldi, et al. 2020. 'The Impact of Biomass Burning and Aqueous-Phase Processing on Air Quality: A Multi-Year Source Apportionment Study in the Po Valley, Italy'. *Atmos. Chem. Phys.* 20: 1233–54. https://doi.org/10.5194/acp-20-1233-2020.

Perrone, Maria Grazia, Maurizio Gualtieri, Luca Ferrero, et al. 2010. 'Seasonal Variations in Chemical Composition and in Vitro Biological Effects of Fine PM from Milan'. *Chemosphere* 78 (11): 1368–77. https://doi.org/10.1016/j.chemosphere.2009.12.071.

Pöschl, Ulrich. 2005. 'Atmospheric Aerosols: Composition, Transformation, Climate and Health Effects'. *Angewandte Chemie International Edition* 44 (46): 7520–40. https://doi.org/10.1002/anie.200501122.

Pye, Liao, Wu, et al. 2009. *Effect of Changes in Climate and Emissions on Future Sulfate-Nitrate-Ammonium Aerosol Levels in the United States*. https://doi.org/https://doi.org/10.1029/2008JD010701.

Ruan, Renhui, Guan Wang, Shuaishuai Li, et al. 2024. 'The Effect of Alkali and Alkaline Earth Metals (AAEMs) on Combustion and PM Formation during Oxy-Fuel Combustion of Coal Rich in AAEMs'. *Energy* 293 (April): 130695. https://doi.org/10.1016/j.energy.2024.130695.

Seinfeld, John H., and Spyros N. Pandis. 2006. *Atmospheric Chemistry and Physics: From Air Pollution to Climate Change*. 2nd ed. J. Wiley.

Shehabi, Arman, Arpad Horvath, William Tschudi, Ashok J. Gadgil, and William W. Nazaroff. 2008. 'Particle Concentrations in Data Centers'. *Atmospheric Environment* 42: 5978−5990. https://doi.org/10.1016/j.atmosenv.2008.03.049.

Stevens, Bjorn, Sandrine Bony, David Farrell, et al. 2021. 'EUREC^4 A'. *Earth System Science Data* 13 (8): 4067–119. https://doi.org/10.5194/essd-13-4067-2021.

Syed, S. 2006. 'Atmospheric Corrosion of Materials'. *Emirates Journal for Engineering Research* 11 (1): 1–24.

Tang, I. N., and K. H. Fung. 1997. 'Hydration and Raman Scattering Studies of Levitated Microparticles: Ba(NO3)2, Sr(NO3)2, and Ca(NO3)2'. *The Journal of Chemical Physics* 106 (5): 1653–60. https://doi.org/10.1063/1.473318.

Tang, Mingjin, Chak K. Chan, Yong Jie Li, et al. 2019. 'A Review of Experimental Techniques for Aerosol Hygroscopicity Studies'. *Atmospheric Chemistry and Physics* 19 (19): 12631–86. https://doi.org/10.5194/acp-19-12631-2019.

Tsimpidi, Alexandra P., Susanne M. C. Scholz, Alexandros Milousis, Nikolaos Mihalopoulos, and Vlassis A. Karydis. 2025. 'Aerosol Composition Trends during 2000–2020: In-Depth Insights from Model Predictions and Multiple Worldwide near-Surface Observation Datasets'. *Atmos. Chem. Phys.* 25: 10183–213. https://doi.org/10.5194/acp-25-10183-2025,%202025.

https://doi.org/10.5194/egusphere-2026-3968
Preprint. Discussion started: 17 August 2026

Wang, Alian, John J. Freeman, and Bradley L. Jolliff. 2009. 'Phase Transition Pathways of the Hydrates of Magnesium Sulfate in the Temperature Range 50°C to 5°C: Implication for Sulfates on Mars'. *Journal of Geophysical Research: Planets* 114 (E4): 2008JE003266. https://doi.org/10.1029/2008JE003266.

Wang, Luntao, Xiong Gao, Hao Zhang, et al. 2025. 'The Corrosion Mechanism of Printed Circuit Boards Affected by Haze Atmospheric Particles'. *RSC Advances* 15: 28439–51. https://doi.org/10.1039/d5ra04326c.

Wang, Y. Zhang, A. Nenes, and C. Fountoukis. 2012. 'Implementation of Dust Emission and Chemistry into the Community Multiscale Air Quality Modeling System and Initial Application to an Asian Dust Storm Episode'. *Atmospheric Chemistry and Physics* 12 (21): 10209–37. https://doi.org/10.5194/acp-12-10209-2012.

Wexler, Anthony S., and Simon L. Clegg. 2002. 'Atmospheric Aerosol Models for Systems Including the Ions H^+, NH_4^+, Na^+, SO_4^{2-}, NO_3^-, Cl^-, Br^-, and H_2O'. *Journal of Geophysical Research: Atmospheres* 107 (D14). https://doi.org/10.1029/2001JD000451.

Zhang, Huanhuan, Wenjun Gu, Yong Jie Li, and Mingjin Tang. 2020. 'Hygroscopic Properties of Sodium and Potassium Salts as Related to Saline Mineral Dusts and Sea Salt Aerosols'. *Journal of Environmental Sciences* 95: 65–72. https://doi.org/https://doi.org/10.1016/j.jes.2020.03.046.

Zieger, P., O. Väisänen, J. C. Corbin, et al. 2017. 'Revising the Hygroscopicity of Inorganic Sea Salt Particles'. *Nature Communications* 8 (1): 15883. https://doi.org/10.1038/ncomms15883.